M del Alamo-Sanza, I Nevares, T Mayr, JA Baro, V Martínez-Martínez, J Ehgartner.
Analysis of the role of wood anatomy on oxygen diffusivity in barrel staves using luminescent imaging
Sensors and Actuators B Chemical Volume 237, December 2016, Pages 1035–1043

Analysis of the role of wood anatomy on oxygen diffusivity in barrel staves using luminescent imaging

María del Alamo-Sanza [a1], *Ignacio Nevares* [a1*], *Torsten Mayr* [b], *Jesus Angel Baro* [a], *Victor Martínez-Martínez* [a], *Josef Ehgartner* [b]
[a]Grupo UVaMOX, E.T.S. Ingenierías Agrarias, Universidad de Valladolid, 34004, Palencia, Spain
[b]Applied Sensors, Institute of Analytical Chemistry and Food Chemistry, Graz University of Technology, 8010 Graz, Austria.
*inevares@iaf.uva.es
[1] These authors contributed equally to this publication

Abstract

This paper explores the use of optical sensors to study the oxygen diffusivity of oak wood staves in wine barrel ageing for four months. 2-D oxygen distribution measurements were performed with planar optodes in combination with a colour RGB camera. The transparency of the optode enables to study the correlation of spatial heterogeneities -due to wood swelling during wetting- in O_2 concentration over the wood surface with data on the different anatomical structures involved. For the first time, oxygen dynamics were described with a resolution that permits the identification of the role of wood anatomy on oxygen permeability/diffusivity.

Keywords

Optical oxygen sensors; oak wood; oxygen diffusivity; barrel; wood anatomy; wine

1. Introduction

Wood used for making wine ageing barrels (cooperage) is mainly from two species of oak: *Quercus alba* (American oak) or *Quercus petraea* (European oak). The choice of species depends on the pursued aromatic and gustatory traits. Wood barrels provide micro-oxygenation of the wine, which is absolutely essential for ageing. Using chemical reactions or electrochemical sensors [1–4], the yearly oxygen transfer rate (OTR) into a barrel to the wine has been measured at 15-28 $mL.L^{-1}$. Recent developments in lifetime-based optical sensors has enabled researchers to measure OTR without modifying oxygen levels [5] or even to measure varying rates, publishing new figures of 10-12 $mg.L^{-1}$ per year [6]. The oxygen flows through the wood, through stave joints, and through the plug [3]. The use of optical sensors together with oximeters has allowed better quantification of oxygen entering the wood, which is now estimated to be more that 50% of total oxygen, depending on wood structure [7].

Oak wood selection in cooperage is based on the concept of grain established by Vivas [8] as the width of the annual growth ring of the tree (for further details about barrel construction see [5]). The choice of fine or very fine grain corresponds to wood of slow growth (annual growth 1 – 2 mm) or very slow growth (annual growth < 1 mm), as the slower the growth, the finer the grain and the higher the porosity and thus the oxygen transfer rate [8–10]. But the relationship between these traits is probably more complex because oxygen diffusion in wood varies greatly among the different anatomical elements (Figure 1A): earlywood, latewood, tyloses, and the type and orientation of medullar rays [6,11,12]. There are just a few references for gas permeability along the longitudinal axis, and it has been estimated to be several thousand times smaller than axial permeability [13]. Recent research using planar sensor optodes and ratiometric analysis of the images allowed to visualize O_2 dynamics within the barrel stave at different moments during wine ageing [14], both in dry and in wet oak wood. In the next step it was also possible to quantify the oxygen gradients inside oak wood and determine the oxygen diffusivity of oak wood depending on the moisture content as a key factor [15]. Wood microstructure plays an important role in wood permeability to oxygen as heterogeneous porous media, and very few data have been published. Although the gas permeability of a porous material is often treated as a constant, this is not true in the case of heterogeneous and/or anisotropic materials. Wood combines these last two conditions; thus, significant variations are observed from sample to sample. Within one and the same species considerable variations are found between different trees; and within one and the same tree there are notable changes between heartwood and sapwood. In these cases, the differences may be attributed to the diverse structural characteristics of the study samples [16]. These are common characteristics in a natural material such as oak wood, whose hardwood is that preferred in cooperage. The hardwood structure in *Quercus* species shows great variation with respect to cell size as well as cell arrangement, being the vessel the distinguishing cell type. Tyloses is usual in European species but greater in American white oak, actually being outgrowths of parenchyma cells through the wall pits into the lumen of vessels. As ring porous species, there are two main types of wood structure in growth annual rings, early- and latewood, the largest pores are in the earlywood while those in the latewood are more evenly distributed and uniform in size.

In the dried state, latewood has a much higher permeability than earlywood, because latewood is much more resistant to pit aspiration, thus the fact that latewood has fewer and smaller pits than earlywood does not lead to lower permeability [17–19]. Besides the differences between early- and latewood, which influence pit aspiration, it should be mentioned that earlywood wets more easily than latewood, because earlywood has a greater roughness and porosity [20,21].

This paper explores the use of optical oxygen sensors to study the structure of wood. 2-D oxygen distribution measurements were performed with planar optodes in combination with a colour RGB camera. The transparency of the optode enables the correlation of spatial

heterogeneities in O_2 concentration over the wood surface and information on the different anatomical structures involved. We present the need for image warp correction as optical planar sensors provide information on non-linear, anisometric moisture-related wood swelling. For the first time, oxygen dynamics were described with a resolution that permits the identification of the role of wood anatomy on oxygen permeability / diffusivity.

2. Material and methods

2.1. Sensor materials

Sensor cocktail containing palladium(II)-5,10,15,20-tetrakis-(2,3,4,5,6- pentafluorphenyl)-porphyrin (PdTPFPP, 3.6 mg), Macrolex Fluorescence Yellow (MY, 5.9) and polystyrene (PS, M = 250 000, 300 mg) in chloroform (4.4 g) was prepared. A Polyethylene terephthalate (PET) nex 506 (thickness: 125 µm) was used as substrate for the sensor foils.

2.2. Transparent planar sensor preparation

The cocktail was knife coated (BYK Drawdown Bar, 3 Mil) on the substrate foil. After drying the sensor foil at 60°C some sensor foils were additionally knife coated (BYK Drawdown Bar, 3 Mil) with a protection cocktail, which contained ELASTOSIL® E4 silicon rubber (1 g) in hexane (3 g).

2.3. Oak wood stave sampling and handling

For this assay, an oak stave from a French oak barrel (*Quercus petraea*) with medium toast and uniform anatomical structure was selected to minimize the variability in the morphological structure. Further, it was required to display ideal splitting, which implies a parallel distribution of the medullar rays with the liquid contact surface of the stave in the barrel. A 40 mm x 70 mm portion with the usual stave thickness of 27 mm was selected and fixed into the device with screws using the minimum pressure necessary to ensure tightness. The fitting of the piece of wood in the setup exposed a section of transverse direction of the oak wood stave to permit direct observation of the tangential flow of oxygen that takes place in oak staves and heads of wine barrels. The planar oxygen sensor was placed in this region and in contact with both the wine and the wood (Figure 1). Additionally, a dissolved oxygen (DO) sensor spot was glued to the centre of the transparent surface of the wine-side chamber.

2.4. Set-up for the barrel scenario simulation

Apparatus for measuring the wood's oxygen permeability typically includes two chambers separated by the wood specimen [10]. Different experimental setups stem from the manner in which the chambers are filled and the initial assay conditions are established. A pressure gradient governed by Darcy's law can be used, and the resulting gas flow is expressed in

$m^3m^{-1}s^{-1}Pa^{-1}$; conversely, the oxygen partial pressure difference at either side of the wood specimen can be considered, constituting a diffusion phenomenon. In the latter case, a molecular flow governed by the first law of Fick is produced, expressed in m^2s^{-1} [18]. This scenario is the predominant situation in barrels because the oxygen partial pressure is much higher than the minimum hydrostatic pressure difference [4]. One of the chambers separated by the wood can be filled with air, and the other with nitrogen, establishing partial pressure gradients of oxygen similar to those produced in an empty barrel [10,22]. To speed up the process, oxygen can be used instead of air, provided the flow rates of oxygen (the donor gas) and nitrogen (the carrier gas) that are driven to the oxygen analyser are maintained constant [10]. This set-up is commonly used for testing the permeability of layers [23–25]. The humidity content of the sample plays a decisive role in the oxygen diffusivity into the wood and must thus be taken into account [17,18,10,22]. Therefore, we developed a device that mimics the scenario of a barrel, with liquid in contact with the toasted interior face of the stave and the opposite face with the atmosphere [15]. This device also maintains the ratio between the interior wood surface and the liquid volume present in the 225-L Bordeaux barrel, see [5] for a full description of the device. DO was monitored by means of a calibrated O_2 optode system sensor (Oxygen Trace spot, PyroScience GmbH, Aachen, Germany) attached to the inner surface of the glass in the device, linked to an optical oxygen meter (FirestingO2, PyroScience GmbH, Aachen, Germany), and was used to determine the DO in wine under the assay conditions and during calibration. One side of the device is composed of glass that performs the DO reading using the optical systems (Figure 1). The device contains a stainless steel tube 40 cm in height with a pressure transducer (Transmitter S-10, Wika, Lawrenceville, GA, USA) that measures and adjusts the hydrostatic pressure to that found in a stave placed at half the height of the barrel.

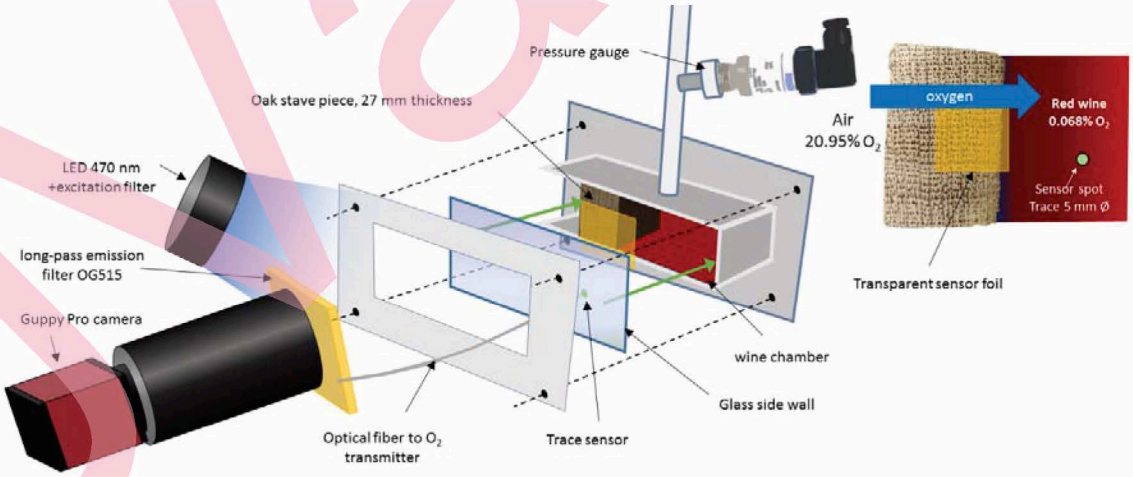

Figure 1: Set-up reproducing the barrel scenario for a piece of full thickness oak stave (27 mm) and the transparent planar sensor placed between the glass and the wood piece along the tangential axis. This configuration allowed us to film the oxygen dynamics and to map dissolved oxygen distribution within the stave thickness over time.

2.5. Imaging

Oxygen imaging was performed using a 470 nm high-power 10 W LED array (www.led-tech.de) as the excitation source. The filter set consisted of an excitation filter BG12 (350-470 nm) and a long-pass emission filter OG515 (515 nm) from Schott (www.schott.com). A Guppy Pro F201C colour camera was used for image acquisition. The camera uses the Sony ICX 274 CCD 1/1.8 image sensor together with a manual zoom lens, 18-108 mm EFL, f/2.5. Image acquisition was performed with a program developed with the LabVIEW 2015 programming platform (National Instruments Corporation http://www.ni.com/labview/), which employed the Vision Development Module together with the AVT driver and VimbaViewer (Allied Vision Technologies GmbH http://www.alliedvision.com). This software allows RGB images to be acquired with different sampling periods, coordinating the operation of the LED array and the camera. Moreover, it performs a pre-processing stage that consists of acquiring several images and averaging them to reduce their signal-to-noise ratio.

2.6. Image analysis

Acquired images were analysed in order to obtain the O_2 concentration for each pixel. To this end, a program based on the LabVIEW 2015 platform and the Vision Development Module was developed to perform the image analysis tasks in the procedure described below. The image analysis can be divided into two stages: the calibration procedure and the processing procedure. We used ratiometric imaging that employed the red and green channels of a colour CCD camera as shown previously [15]. The oxygen-sensitive emission of sensor foils was detected in the red channel, while the emission of a reference dye was detected in the green channel. This measurement setup allowed for accurate, real-time 2-dimensional (2D) oxygen imaging of superior quality compared to intensity imaging.

The first stage is the calibration procedure, which consists of calculating the coefficients of a Stern-Volmer model that best fit the performed experiments [26,27]. The procedure involved arranging a set of images of the sensor under known O_2 concentrations. Each image was filtered with a mean filter using a 3x3 pixel mask, filtering the red, green and blue channels separately. After that, the RGB filtered images were transformed to ratiometric images by dividing the red and the green values for each pixel. A set of mean ratiometric values of a region of 100x100 pixels was calculated with the images, creating the calibration curve, fitted with a function that modelled the O_2 concentration value versus the inverse of the mean ratiometric value and normalized to have a ratiometric mean value of 1 for O_2=0%. The *Nonlinear curve fit.vi* function of LabVIEW was employed to obtain the constant values of the Stern-Volmer model that best fit the calibration curve using the Levenberg-Marquardt algorithm.

The second stage is the processing procedure, which transforms a set of acquired images into colour mapped images of O_2 concentration levels, applying the Stern-Volmer model with the coefficients previously obtained in the calibration procedure. The image processing procedure consisted of two steps. In the first step, ratiometric images were calculated in the same way as in the calibration procedure, and in the second step we obtained the O_2 concentration image applying the Stern-Volmer model.

Finally, the developed program included a procedure to calculate the mean O_2 value in a region of interest (ROI) defined by the user.

2.7. Experimental protocol

The device chamber was tested for air tightness by fixing a metal piece shaped as the wood specimen to the device. This chamber was filled with N_2, and the DO signal was monitored for 24 h. The pressure was simultaneously monitored with a pressure transducer. Once device tightness was confirmed, and prior to the assay, the accuracy of the planar transparent oxygen sensor in contact with the air (i.e. at 100% air saturation) was verified with the device chamber full of atmospheric air under the conditions of a climate-controlled barrel room (15±1°C, 75-80% humidity). All the air was then displaced with X50 nitrogen (99.9992% Carburos Metálicos, Spain), and the device was maintained under these conditions for at least twelve hours to ensure gradual degassing of the wood from the internal to the external side of the oak stave. Immediately afterwards, the device chamber was filled with red wine of the Tempranillo variety. The use of wine has additional implications, since the rapid consumption of oxygen by the wine establishes a gradient of DO concentrations under the driving force of the incoming diffused oxygen. In order to mimic the conditions under which an increased oxygen transfer takes place in a barrel [2,28], the pressure inside the wine side of the chamber was adjusted with a syringe to a pressure of -100 hPa in the system's head space (the upper part of the tube, in the vicinity of the pressure transducer). This is within pressure levels commonly found inside wine aging barrels [29]. The wood specimen was studied for 127 days, and its DO content distribution within the thickness of the stave was subsequently analysed over different time periods, allowing the moisture content to increase in the wood. This procedure ensured that the partial pressure gradient of oxygen inside and outside the device never fell below 90% of the gradient found in a barrel [30]. The assays were performed in a climate-controlled barrel room (15±1 °C, 75-80% humidity).

The software application was programed to capture images at ten minute intervals during the first days and twice a day after the first two weeks. Time points were alternated with those of the DO measurements with the luminescent system to avoid interference. These readings allowed us to monitor the oxygen that diffused towards the liquid from the atmospheric air and to monitor the oxygen content distribution within the wood under different humidity contents.

DO level analysis was performed using ANOVA tests using the STATISTICA program (version 8.0, 1984–2007; StatSoft, Tulsa, OK, USA)

3. Results and discussion

In this study, we evaluate the possibility of 2D-imaging the O_2 distribution across the thickness of an oak stave in a barrel scenario. Our setup incorporated a DO sensor over the complete surface, side to side from the atmosphere to the wine (Figure 1). Special care was taken to avoid interference due to the circular disposition of the LEDs around the lens in the camera that resulted in a better signal to noise ratio in the middle of the image [14].
At the start of the experiment the Moisture Content (MC) of the barrel wood was 12-14%, which corresponds to 43-48% porosity. During ageing, the wine-wood interface is soaked and the oxygen present in any porous structure is either completely taken or displaced by wine. In order to ensure that our transparent planar sensor fulfilled this requirement, we generated a calibration curve from 0 to 100% Air sat. The obtained calibration showed the expected exponential decay over the relevant O_2 concentration range [31] (Figure 2).

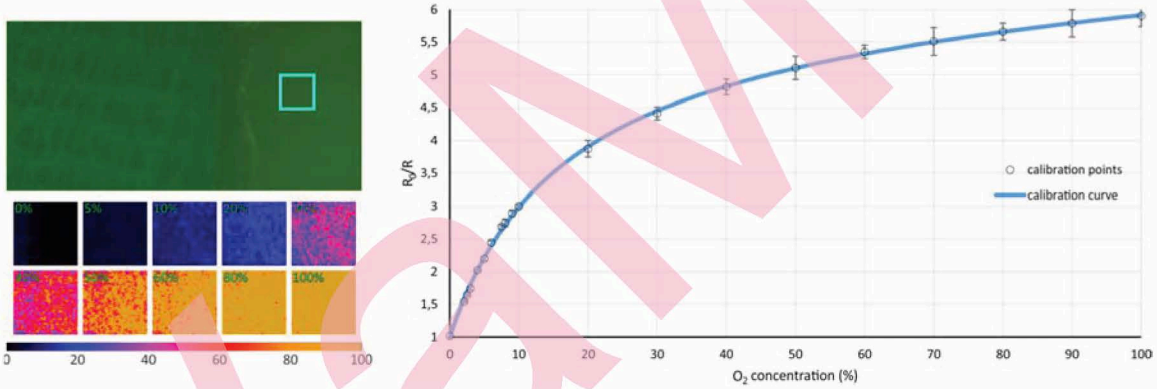

Figure 2: A) False colour images representing the % air sat. obtained from ratiometric images (ratio between the red and green channel extracted from RGB images) of liquid at various defined O_2 levels in wine side chamber. (B) A calibration curve calculated by fitting the Stern-Volmer model ($R^2 > 0.999$) to the R_0/R values vs. O_2 concentration data obtained from the region of interest (ROI) highlighted in (A), where R is the red/green ratio and R_0 is the value of R for O_2=0%. Symbols and error bars represent means ± 5*standard deviation; n = 5.

Planar transparent sensor foils, under complete air-tight adhesion to the glass window and to the transversal section of a wood stave, permit exclusive measurement of the oxygen flux along the transversal axis from the outside to the wine contained in the barrel. A very thin layer of silicon applied between the wood and the sensor foil avoided infiltration of any fluid (wine or air) and allowed for a flexible bond to ensure wood swelling under soaking.

An initial observation of the acquired images over 18 weeks showed that the transparency of the sensor allows identification in the images of different types of wood structures such as the rays. Moreover, a preliminary analysis of the images showed the swelling of wood due to its soaking with the wine of the barrel. It can be seen in Figure 3, which displays one image

captured at the initial stages and another of the last stages of the experiment. A swelling of 4.0% was estimated on the horizontal axis with measurements of distances between rays along the tangential axis of the staves. This value is common for *Quercus petraea* when toasted in cooperage [32,33]. The vertical axis did not suffer appreciable swelling because the piece of wood was firmly clamped by the device, and the thickness axis was also strongly fixed, exactly as happens in a production barrel stave.

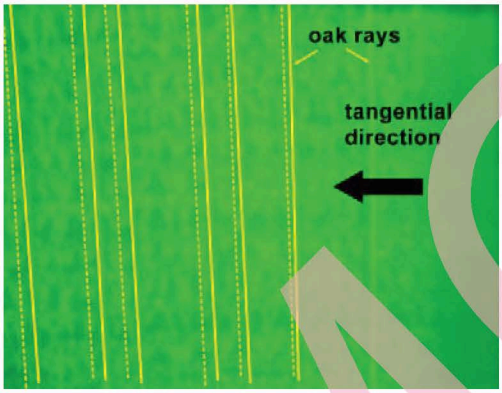

Figure 3: Detail of the initial (hard line) and last (dash line) RGB images of the experiment with medullar oak rays highlighted in yellow. The images were histogram-adjusted to better appreciate wood swelling.

The swelling of the piece of wood caused subsequent analysis of the different regions of interest (ROIs) to be done considering this displacement. The ROIs were chosen using the first image of the set as a reference, and the distortion on the horizontal axis was calculated for each ray on the set of photographs. This information was used to recalculate the coordinates of the ROIs.

In this context, electrochemical micro sensors are not adequate for measuring oxygen at a range of depths because wood is a hard, complex matrix and atmospheric oxygen may reach the sensor [34]. As an additional advantage over traditional spot sensors, planar sensors permit the capture of 2D images of the O_2 distribution across the whole section of the stave [35]. The application to the study of the process of oxygen entry through oak wood in a barrel with wine allows us to explore the heterogeneity in O_2 concentration and the mapping of O_2 dynamics over the full thickness of barrel staves without disturbing the original processes. An 18-week time frame for the oxygen levels across the transversal section of the barrel stave allowed us to reveal the dynamics of oxygen diffusion in different regions (Figure 4, zone I, II, III). We observed that zone III, located closest to the wine, consistently showed the lowest oxygen levels as it was the furthest from the atmosphere; second was zone II, located 9 mm away from the wine; and then zone I, furthest from the wine, showed the highest levels of O_2 during most of the study (Figure 4). Two months into ageing, zone I showed oxygen saturation levels while most of the wood was around 50% Air sat.

These results confirm previous findings [15] on the role of moisture content in reduced oxygen diffusivity that causes its accumulation in the driest sector of the wood. Around week

11 (Figure 4G), zone I displays a large increase in oxygen content caused by reduced diffusivity in zones II and III, soaked in wine at this stage. It is noted that the oxygen accumulates in zone I because accessed with difficulty to zones II and III of wood.

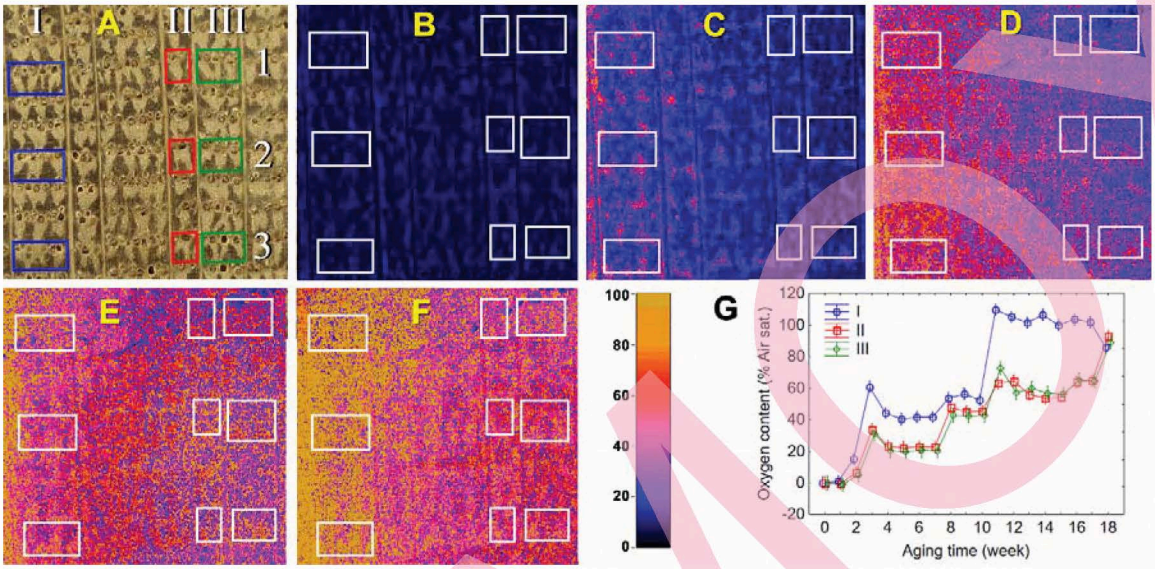

Figure 4. Location of wood zones I, II & III (A); initial DO distribution within studied region (B); after 2 weeks (C); After 5 weeks (D); after 9 weeks (E); after 14 weeks (F) and Oxygen flux through wood: from atmosphere towards wine (G).

The images of O_2 concentration over the transparent planar optode unmistakably showed heterogeneity in O_2 concentration that correlated with different anatomical structures of the wood. It was explored in two regions with different growth rates as defined in the subjective classification of wood for cooperage: a first region of 3 mm^2 of slow growth (1 $mm.y^{-1}$) with 3 yearly growth rings labelled "1" in figure 5; a second zone of the same size and faster growth (1.5 $mm.y^{-1}$) with 2 yearly growth rings labelled "2" in figure 5. All oxygen content is expressed as departures from the initial value.

Figure 5 shows the analysis of average oxygen content of these two regions during the 18 weeks of ageing. Dissolved oxygen levels significantly grow with ageing time ($p=0.000$) at almost the same rate in both regions. We observed that the region of higher growth showed consistently higher oxygen levels than the region of slower growth ($p=0.0567$), and the difference was much greater after week 11. We conclude that the faster the growth, the faster the oxygen flows across the wood. Coarse grain wood leads to higher oxygenation of wine than fine grained wood, which grows more slowly.

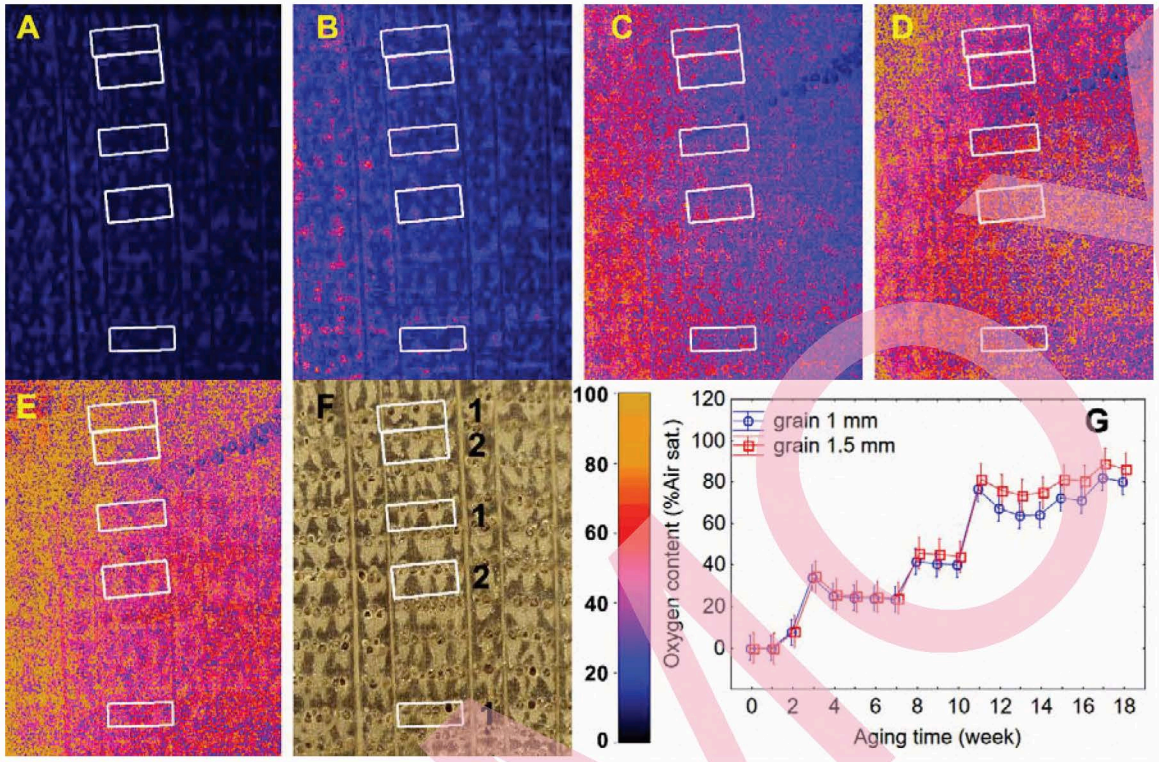

Figure 5. Images of colour mapped O_2 levels: initial (A), week 2 (B), week 5 (C), week 9 (D), week 14 (E), key for growth zones 1 (1mm) and 2 (1.5mm) (F), and oxygen dynamics (G)

In order to evaluate the spatial resolution of the method, we investigated the fine-scale distribution of O_2 over a few microstructure elements. A single stretch of wood, located between two medullar rays located 6.5 and 9 mm away from the wine, was inspected to identify late- and earlywood within the yearly growth rings (Figure 6). The stretch covered 27.78 mm^2 (2.5 mm x 11.1 mm) and comprised 8 growth rings (Table 1). Yearly growths ranged from 1.15 to 1.79 mm with average 1.39 mm, 0.55 mm of earlywood and 0.84 latewood. In terms of length, the stretch was 11.1 mm long with 6.73 mm (60.6%) of late wood and 4.37 mm (39.4%) of earlywood: a ratio of 1.5 of late over earlywood.

Table 1.- Mean structural characteristics of 8 growth rings inside the piece of French oak wood studied.

Ring number	Grain (mm)	Earlywood width EW (mm)	Latewood width LW (mm)	Texture (%)	EW (%)
1	1.20	0.54	0.66	55.1%	44.9%
2	1.37	0.58	0.79	57.7%	42.3%
3	1.44	0.53	0.91	63.1%	36.9%
4	1.24	0.42	0.82	66.1%	33.9%
5	1.79	0.70	1.09	61.0%	39.0%
6	1.15	0.44	0.71	61.4%	38.6%
7	1.32	0.57	0.74	56.3%	43.7%

8	1.59	0.57	1.03	64.4%	35.6%
Mean	1.39	0.54	0.84	60.6%	39.4%
SD	0.22	0.09	0.15	3.9%	3.9%

Grain (mm), calculated as the sum of the width of early wood (EW, mm) and late wood (LW, mm); Texture (%) calculated as the width of late wood (mm) divided by the grain (mm); proportion of early wood (EW%) in the rings calculated as the distance (mm) of early wood divided by the grain (mm).

We found that oxygen entering the observed zone increased with time during the ageing period of 18 weeks and ranged from 80 to 100%, with no significant differences among rings (p=0.7211) (Figure 6A). In every ring, the oxygen level change showed very similar patterns from 0% Air sat. to 60-90% Air sat. at week 18.

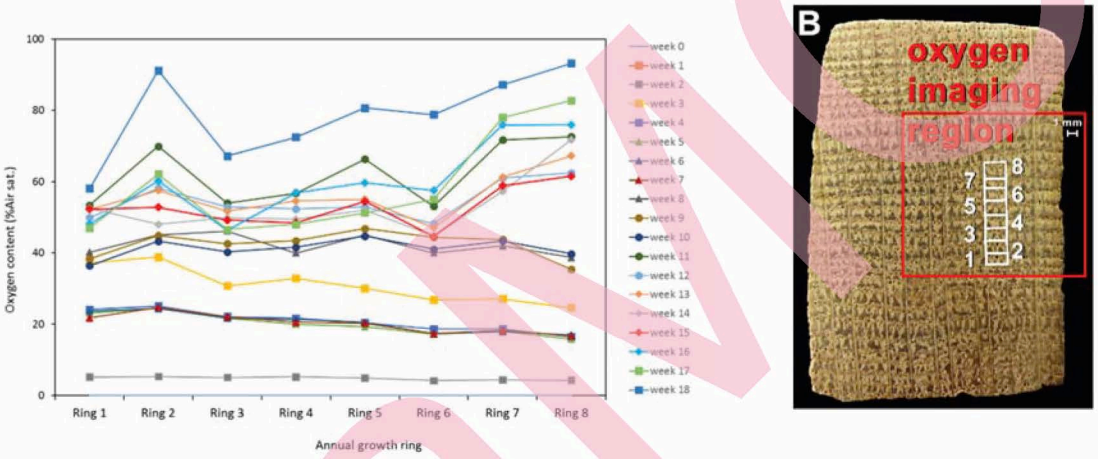

Figure 6. Average oxygen evolution (%Air sat.) during the 18-week wine ageing in a set of 8 yearly growth rings (A) and key for the localization of the eight annual growth rings studied in the oak stave (B).

We could clearly visualize how O_2 concentration varied across individual microstructure elements within each of the annual growth rings showing the high spatial resolution of the transparent planar optode together with the camera. This enhanced resolution enables visualization of the differences in oxygen diffusivity of the microstructures that contribute to a total diffusivity higher than expected and increasing over time to 78% Air sat. Figure 7 represents the mean DO level evolution in latewood, earlywood and in the annual growth ring calculated according to the percentage of each kind of wood measured in each annual growth ring (Table 1).

Besides imaging steady state O_2 concentrations, the method presented here also enables the mapping of O_2 dynamics over wood microstructure elements. We observed that oxygen reaches successive growth rings through late and earlywood. Our results show that the flow through latewood is significantly greater than that flowing through earlywood (p=0.000). This difference holds for the whole of the 18 weeks of the ageing period, with significant differences after the second week. Latewood has a bigger role in oxygen transfer and thus woods with high growth rates, with coarser grain, lead to greater wine oxygenation.

This is in sharp contrast to a study by Vivas et al. [10], performed with a set of pieces of dry wood of several thicknesses (2, 4, 8 mm) and types of grain (coarse and fine). They concluded that fine grained wood lets oxygen diffuse better than coarse grained wood. Such differences may be attributed to the very different thicknesses being considered (2, 4, and 8 mm vs. 27 mm), and for much shorter time lapses (less than 5 days vs. the complete ageing of 18 weeks) and with different fluid interfaces (gas at both sides vs. gas and liquid). Our set up reproduces the wine filled barrel working scenario much more closely. Other studies [17–19] have already described higher permeability in dry latewood than in earlywood, because latewood is much more resistant to pit aspiration, thus the fact that latewood has fewer and smaller pits than earlywood does not lead to lower permeability [17–19]. Besides differences between early- and latewood, which influence pit aspiration, it should be mentioned that earlywood soaks more easily than latewood, because earlywood has greater roughness and porosity [20,21].

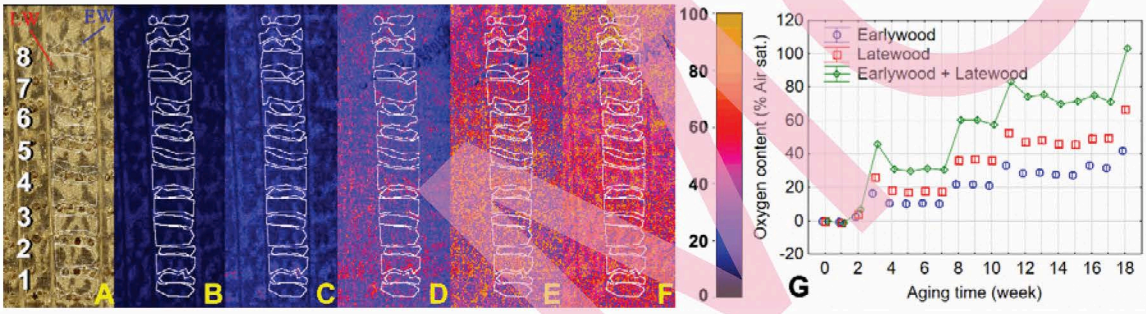

Figure 7. Key for growth zones EW and LW (A); initial stage (B); after 2 weeks (C); After 5 weeks (D); after 9 weeks (E); after 14 weeks (F) and Average O_2 evolution for the latewood (LW-red); earlywood (EW-blue) and both together in the eight selected annual growth rings (Table 1) for the 18 monitored weeks (G).

4. Conclusion

We present an application for transparent planar oxygen sensors for visualizing the distribution of O2 concentration and dynamics across the section of oak staves in a barrel scenario with ratiometric imaging and a RGB camera. We explored such dynamics at high spatial-temporal resolution over areas ranging from several mm^2 to individual portions of annual growth rings. This technique allowed us to see for the first time how O_2 diffuses in different microstructure elements of wood, and to analyse the oxygen dynamics in different kinds of wood considering the grain size classification commonly used in cooperage. The transparent nature of the planar sensor allowed us to take into account the swelling of the wood with increased MC in a simple setup, avoiding a much more complex one based on referenced points in the planar sensor, quite difficult to achieve in typically opaque sensor films due to the high anisometry of the studied surface.

Funding

This work was supported by FEDER founds, Junta de Castilla y León (VA124U14, VA028U16) and MINECO (AGL2014-54602P). The authors declare no competing financial interest.

Contributors

M.A.S. and I.N. designed the research. T.M and J.E. developed the sensors; M.A.S. and I.N. conducted experiments. J.A.B. and V.M. analysed the images. MAS and IND analysed the data and wrote the manuscript with editorial help from J.A.B. and V.M. All authors have given approval to the final version of the manuscript.

References

[1] J. Ribereau-Gayon, Contribution à l'étude des oxydations et réductions dans les vins, Université de Bordeaux, 1933.

[2] M. Moutounet, J.P. Mazauric, B. Saint-Pierre, J.P. Micaleff, J. Sarris, Causes et conséquences de microdèformations des barriques au cours de l'élevage des vins, Rev. Des Oenologues. (1994) 34–39.

[3] N. Vivas, Y. Glories, Modélisation et calcul du bilan des apports d'oxygène au cours de l'élevage des vins rouges. II. Les apports liés au passage d'oxygène au travers de la barrique, Progrès Agric. Vitic. 114 (1997) 315–316.

[4] M. Kelly, D. Wollan, Micro-oxygenation of wine in barrels, Aust. New Zeal. Grapegrow. Winemak. 473a (2003) 29–32.

[5] I. Nevares, M. del Alamo-Sanza, Oak stave oxygen permeation: A new tool to make barrels with different wine oxygenation potentials, J. Agric. Food Chem. 63 (2015) 1268–1275.

[6] M. del Alamo-Sanza, I. Nevares, Recent advances in the evaluation of the oxygen transfer rate in oak barrels, J. Agric. Food Chem. 62 (2014) 8892–8899.

[7] I. Nevares Domínguez, M. del Álamo Sanza, Oxygène et barriques: Actualisation des connaissances Quantité et voies de pénétration de l'oxygène dans la barrique, Rev. des oenologues des Tech. Vitivinic. oenologicques Mag. Trimest. d'information Prof. 41 (2014) 41–44.

[8] N. Vivas, The notion of grain in cooperage, J. Des Sci. Tech. La Tonnellerie. 1 (1995) 17–32.

[9] F. Feuillat, F. Huber, Keller, Mise Au Point Sur: La notion de grain utilisee pour le classement des merrains de chene (Quercus Robur L., Quercus Petraea Liebl.), Rev. Française D'oenologie. 32 (1992) 65–69.

[10] N. Vivas, H. Debeda, F. Menil, N. Vivas de Gaulejac, M.F. Nonier, Mise en évidence du passage de l'oxygène au travers des douelles constituant les barriques par l'utilisation d'un dispositif original de mesure de la porosité du bois. Premiers résultats, Sci. Aliments. 23 (2003) 655–678.

[11] M.M. Guillaume de Pracomtal, R. Teissier du Cros, A.-C. Monteau, Types of oak grain, wine élevage in barrel, Pract. Winer. Vineyard. (2014) 64–69.

[12] F. Feuillat, R. Keller, Variability of oak wood (Quercus robur L., Quercus petraea Liebl.) anatomy relating to cask properties, Am. J. Enol. Vitic. 48 (1997) 502–508.

[13] S. Kumar, K. Kohli, Some aspects of fluid flow in wood. 4: gas permeability studies in hardwoods, J. (Timber Dev. Assoc. India). 34 (1988) 5–22.

[14] I. Nevares, R. Crespo, C. González, M. del Alamo-Sanza, Imaging of oxygen permeation in the oak wood of wine barrels using optical sensors and a colour camera, Aust. J. Grape Wine Res. 20 (2014) 353–360.

[15] I. Nevares, T. Mayr, J.A. Baro, J. Ehgartner, R. Crespo, M. del Alamo-Sanza, Ratiometric oxygen imaging to predict oxygen diffusivity in oak wood during red wine barrel aging, Food Bioprocess Technol. 9 (2016) 1049–1059.

[16] A.J. Miyara, V. Costanza, Gas flow in hardwoods, Wood Sci. Technol. 25 (1991) 289–299.

[17] J.F. Siau, I. Wood--influence of moisture on physical properties, Dept. of Wood Science and Forest Products, Virginia Polytechnic Institute and State University, [Blacksburg, VA], 1995.

[18] J.F. Siau, Transport processes in wood, Springer-Verlag, Berlin ; New York, 1984.

[19] C. Hansmann, W. Gindl, R. Wimmer, Permeability of wood - a review , Wood Res. 47 (2002) 1–16.

[20] G.I. Mantanis, R. a. Young, Wetting of wood, Wood Sci. Technol. 31 (1997) 339–353.

[21] M. Scheikl, M. Dunky, Measurement of dynamic and static contact angles on wood for the determination of its surface tension and the penetration of liquids into the wood surface, Holzforschung. 52 (1998) 89–94.

[22] J. Sorz, P. Hietz, Gas diffusion through wood: implications for oxygen supply, Trees - Struct. Funct. 20 (2006) 34–41.

[23] ASTM, D3985 - 05. Standard test method for oxygen gas transmission rate through plastic film and sheeting using a coulometric sensor, 15.10 (2005).

[24] ASTM, F1307 - 02. Standard test method for oxygen transmission rate through dry packages using a coulometric sensor, 15.10 (2007).

[25] ASTM, F1927 - 07. Standard test method for determination of oxygen gas transmission rate, permeability and permeance at controlled relative humidity through barrier materials using a coulometric detector, 15.10 (2007).

[26] H. Tschiersch, G. Liebsch, A. Stangelmayer, L. Borisjuk, H. Rolletschek, Planar oxygen sensors for non invasive imaging in experimental biology, Intech Europe, Rijeka, Croatia, 2011.

[27] K. Koren, S.L. Jakobsen, M. Kühl, In-vivo imaging of O2 dynamics on coral surfaces spray-painted with sensor nanoparticles, Sensors Actuators B Chem. (2016).

[28] M. Moutounet, J.P. Mazauric, B. Saint-Pierre, J.F. Hanocq, Gaseous exchange in wines stored in barrels, J. Des Sci. Tech. La Tonnellerie. 4 (1998) 131–145.

[29] R.G. Peterson, Formation of reduced pressure in barrels during wine aging, Am. J. Enol. Vitic. 27 (1976) 80–81.

[30] O.G. Piringer, Permeation of gases, water vapor and volatile organic compounds, in: O.G. Piringer, A.L. Baner (Eds.), Plast. Packag. Mater. Food Barrier Funct. Mass Transp. Qual. Assur. Legis., Wiley-VCH, Weinheim ; New York, 2000: p. 250.

[31] X. Wang, O.S. Wolfbeis, Optical methods for sensing and imaging oxygen: materials, spectroscopies and applications., Chem. Soc. Rev. 43 (2014) 3666–761.

[32] Jan .F. Rijsdijk, Peter B. Laming, Physical and Related Properties of 145 Timbers: Information for practice, Dordrecht: Springer, London, 2011.

[33] R. Popper, P. Niemz, G. Eberle, Untersuchungen zum Sorptions- und Quellungsverhalten von thermisch behandeltem Holz, Holz Als Roh- Und Werkst. 63 (2005) 135–148.

[34] D. Gansert, M. Burgdorf, R. Lösch, A novel approach to the in situ measurement of oxygen concentrations in the sapwood of woody plants, Plant. Cell Environ. 24 (2001) 1055–1064.

[35] M. Staal, S.M. Borisov, L.F. Rickelt, I. Klimant, M. Kühl, Ultrabright planar optodes for luminescence life-time based microscopic imaging of O2 dynamics in biofilms, J. Microbiol. Methods. 85 (2011) 67–74.